

Electronic Supplementary Information

Multicomponent crystals of nitrofurazone – when more is less

Kudzaishe Nigel Sharara^a, Kudzanai Nyamayaro^a, Merrill M. Wicht^a,
Gerhard A. Venter^b and Nikoletta B. Báthori^{a*}

^a *Department of Chemistry, Cape Peninsula University of Technology, P.O.Box 652, Cape Town, 8000, South Africa.*

^b *Scientific Computing Research Unit and Department of Chemistry, University of Cape Town, Rondebosch 7701, South Africa.*

Corresponding author: Nikoletta B. Báthori, E-mail: bathorin@cput.ac.za; Fax: +27 21 460 3854; Tel: +27 21 460 8354

Table of Content

Schemes

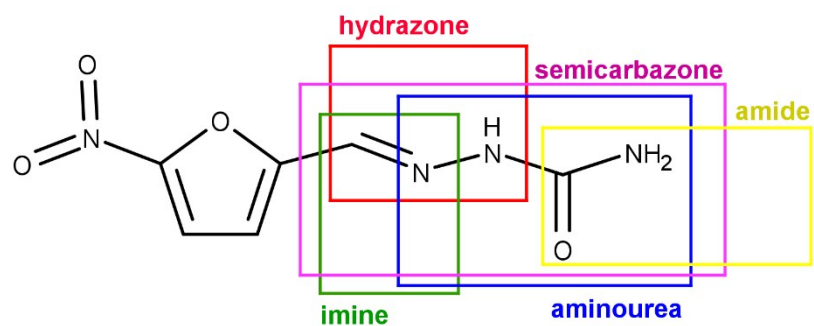
Scheme S1	The semicarbazone chain with subgroups representing the multipotent nature of NFZ in hydrogen bond formation.	3
Scheme S2	CSD hits for the selected semicarbazone fragments.	4
Scheme S3	Hits obtained from the hydrogen bond motif search, where X is any atom.	5

Tables


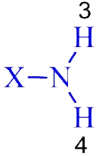
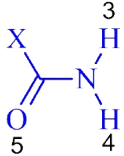
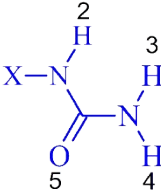
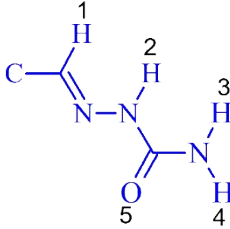
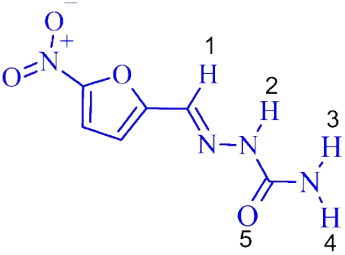
Table S1	List of solvents/co-formers applied in cocrystallization experiments.	6
Table S2	Crystallographic data of the three polymorphic forms of NFZ collected at low (LT) or room temperature (RT).	7
Table S3	List of acid solvents used and their respective crystallizations.	8
Table S4	Crystallographic data of the three multicomponent crystals of NFZ.	9
Table S5	The geometric parameters for intermolecular interactions in $4\text{NFZ}\cdot[\text{H}_3\text{O}^+][\text{ClO}_4^-]$.	11
Table S6	The geometric parameters for intermolecular interactions in $\text{NFZ}\cdot\text{H}_3\text{PO}_4$.	12
Table S7	Hydrogen bonds in $\text{NFZ}\cdot\text{PA}$.	12
Table S8	Torsion angles of NFZ in polymorphs α , β and γ and in MCCs.	14
Table S9	Relevant torsion angles and their resulting conformation (continued to next pages).	15

Figures

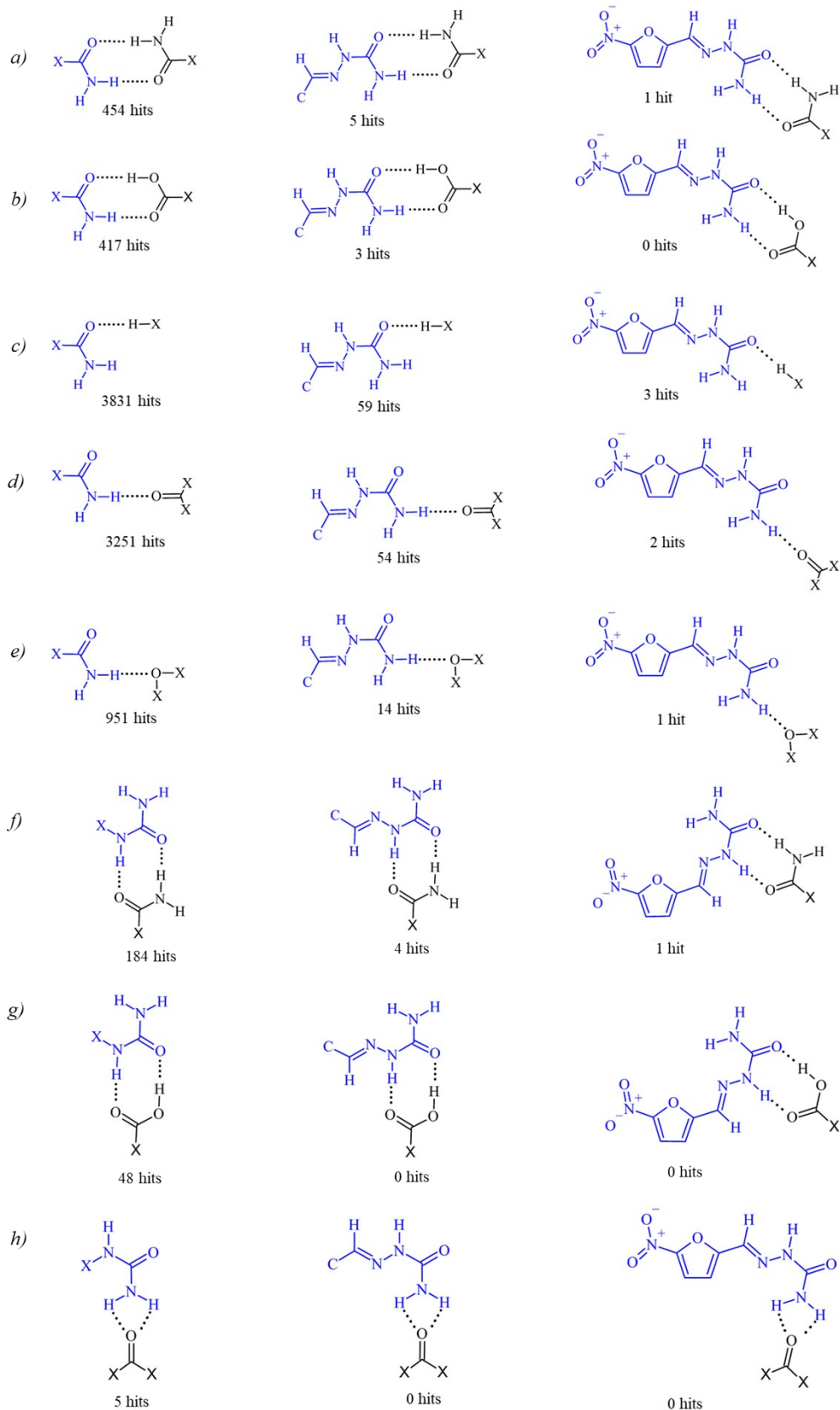
Figure S1	Hydrogen bonds between the NFZ molecules in the 3 reported polymorphs.	8
Figure S2	Photograph of uncut $4\text{NFZ}\cdot[\text{H}_3\text{O}^+][\text{ClO}_4^-]$ co-crystal salt.	10
Figure S3	An uncut crystal of $\text{NFZ}\cdot\text{H}_3\text{PO}_4$.	10
Figure S4	An uncut crystal of $\text{NFZ}\cdot\text{PA}$.	10
Figure S5	Interaction energies of fragments taken from the crystal structure and used without further optimization. Calculations done at the DSD-PBEP86/def2-QZVPP level of theory, corrected for BSSE using the counterpoise procedure.	13
Figure S6	Interaction energies of the amide-PPA synthons after geometry optimization. Calculations done at the DSD-PBEP86/def2-QZVPP//PBE0-D3(BJ)/def2-TZVP level of theory, corrected for BSSE using the counterpoise procedure.	13
Figure S7	Eight possible conformers arising from the <i>sp</i> and <i>ap</i> torsion combinations. Newly found conformer of NFZ in $\text{NFZ}\cdot\text{H}_3\text{PO}_4$ crystal is circled in red.	14
Figure S8	Relative conformational energies, calculated at the DSD-PBEP86/def2-QZVPP//PBE0-D3(BJ)/def2-TZVP level of theory.	15
Figure S9	PXRD patterns of the samples prepared with different methods of $4\text{NFZ}\cdot[\text{H}_3\text{O}^+][\text{ClO}_4^-]$.	21
Figure S10	PXRD patterns of the samples prepared with different methods of $\text{NFZ}\cdot\text{H}_3\text{PO}_4$.	22
Figure S11	PXRD patterns of the samples prepared with different methods of $\text{NFZ}\cdot\text{PA}$.	22
Figure S12	DSC curves of $4\text{NFZ}\cdot[\text{H}_3\text{O}^+][\text{ClO}_4^-]$ bulk material and samples obtained from LAG.	23
Figure S13	Thermal analysis curve showing steps of mass loss of $4\text{NFZ}\cdot[\text{H}_3\text{O}^+][\text{ClO}_4^-]$.	23
Figure S14	DSC curve of $\text{NFZ}\cdot\text{H}_3\text{PO}_4$ bulk material and $\text{NFZ}\cdot\text{H}_3\text{PO}_4$ LAG.	24
Figure S15	Thermal analysis curve showing weight loss in $\text{NFZ}\cdot\text{H}_3\text{PO}_4$ bulk material.	24
Figure S16	DSC and DTA curves of $\text{NFZ}\cdot\text{PA}$.	25
Figure S17	FTIR spectra of NFZ and $4\text{NFZ}\cdot[\text{H}_3\text{O}^+][\text{ClO}_4^-]$.	26
Figure S18	FTIR spectra of NFZ and $\text{NFZ}\cdot\text{H}_3\text{PO}_4$.	27
Figure S19	FTIR spectra of NFZ and $\text{NFZ}\cdot\text{PA}$.	28



Scheme S1. The semicarbazone chain with subgroups representing the multipotent nature of NFZ in hydrogen bond formation.

Fragment	Bonding sites	CSD Hits
	1	189723
	2	35894
	3	4245
	4	829
	5	60
	5	3

Scheme S2. CSD hits for the selected semicarbazone fragments.



Scheme S3. Hits obtained from the hydrogen bond motif search, where X is any atom.

Table S1. List of solvents/co-formers applied in cocrystallization experiments.

Solvent/Co-former	Molecular formula	Polarity index	Dielectric constant (ϵ)	Outcome
			$\epsilon_{\text{vacuum}}=1$	
acetamide:acetonitrile	$\text{C}_2\text{H}_5\text{NO}:\text{C}_2\text{H}_3\text{N}$	-	-	β -polymorph
acetonitrile	$\text{C}_2\text{H}_3\text{N}$	5.8	37.5	β -polymorph
acetone	$\text{C}_3\text{H}_6\text{O}$	5.1	21.5	α -polymorph
aspirin- isopropanol: H_2O (2:1)	$\text{C}_9\text{H}_8\text{O}_4:\text{C}_3\text{H}_8\text{O}:\text{H}_2\text{O}$	-	-	β -polymorph
1,4-dioxane	$\text{C}_4\text{H}_8\text{O}_2$	4.8	2.0	β -polymorph
2-aminopyridine:isopropanol	$\text{C}_5\text{H}_6\text{N}_2:\text{C}_3\text{H}_8\text{O}$	-, 3.9	-, 18.0	γ -polymorph
2-aminopyridine:ethanol	$\text{C}_5\text{H}_6\text{N}_2:\text{C}_2\text{H}_6\text{O}$	-, 5.2	-, 16.2	β -polymorph
2,3-lutidine	$\text{C}_7\text{H}_9\text{N}$	-	-	β -polymorph
2-picoline	$\text{C}_6\text{H}_7\text{N}$	9.8	-	γ -polymorph
3,4-lutidine	$\text{C}_7\text{H}_9\text{N}$	-	-	β -polymorph
4-picoline	$\text{C}_6\text{H}_7\text{N}$	-	-	β -polymorph
N,N-dimethylacetamide	$\text{C}_3\text{H}_6\text{O}$	6.5	-	β -polymorph
N,N-dimethylformaldehyde	$\text{C}_3\text{H}_7\text{NO}$	6.4	-	β -polymorph
isopropanol	$\text{C}_3\text{H}_8\text{O}$	3.9	18.0	γ -polymorph
methylethylketone	$\text{C}_3\text{H}_6\text{O}$	4.7	-	β -polymorph
methanol	CH_4O	5.1	33.0	α -polymorph
pyridine	$\text{C}_5\text{H}_5\text{N}$	5.3	13.2	possible inclusion compound
tetrahydrofuran	$\text{C}_4\text{H}_8\text{O}$	4.0	-	β -polymorph
formic acid	HCOOH		$pK_a= 3.75$	β -polymorph
acetic acid	CH_3COOH		$pK_a= 4.76$	β -polymorph
propanoic acid	$\text{C}_2\text{CH}_3\text{COOH}$		$pK_a= 4.85$	solvate

Table S2. Crystallographic data of the three polymorphic forms of NFZ collected at low (LT) or room temperature (RT).

	α -RT	β -RT	β -LT	γ -RT	γ -LT
Refcode	WERVEU	WERVEU01	-	WERVEU02	-
Formula	C ₆ H ₆ N ₄ O ₄	C ₆ H ₆ N ₄ O ₄	C ₆ H ₆ N ₄ O ₄	C ₆ H ₆ N ₄ O ₄	C ₆ H ₆ N ₄ O ₄
Mr	198.15	198.15	198.15	198.15	198.14
Temp (K)	295	295	173	295	173
System	Monoclinic	Monoclinic	Monoclinic	Monoclinic	Monoclinic
Group	<i>P</i> 2 ₁ / <i>a</i>	<i>P</i> 2 ₁	<i>P</i> 2 ₁	<i>P</i> 2 ₁ / <i>c</i>	<i>P</i> 2 ₁ / <i>c</i>
a/Å	9.943(1)	4.1964(3)	4.2098(5)	13.5703(6)	13.4449(14)
b/Å	8.402(1)	7.0129(5)	6.9632(9)	7.8254(3)	7.8221(9)
c/Å	10.220(1)	14.4528(10)	14.2021(18)	7.9677(4)	7.8587(9)
α/°	90	90	90	90	90
β/°	101.18(1)	90.924(7)	92.360(3)	102.260(4)	103.134(3)
γ/°	90	90	90	90	90
Vol. /Å³	837.587	425.28(5)	415.96(9)	804.859	804.86(16)
Z	4	2	2	4	4
ρ (gcm⁻³)	1.571	1.547	1.582	1.592	1.635
μ (mm⁻¹)	0.126	0.13	0.135	0.14	0.140
Dataset (<i>hkl</i>)	-13,13;-11,11;0,13	-5,5;-7,9;-19,19	-5,5;-9,9;-18,18	-18,17;-10,10;-10,10	-16,17;-10,10;-10,10
F(000)	408	204	204	408	408
Crystal size (mm)	-	0.24 x 0.22 x 0.16	0.08 x 0.17 x 0.41	0.31 x 0.27 x 0.22	0.25 x 0.25 x 0.1
Radiation [Å]	MoK α , 0.7107	MoK α , 0.71073	MoK α , 0.71073	MoK α , 0.71073	MoK α , 0.71073
Theta min-max [°]	2.03, 27.50	2.8, 29.4	1.435, 28.033	3.0, 29.4	3.034, 28.423
Final R indices [I>2.0 (I)]		R ₁ = 0.032 wR ₂ = 0.059	R ₁ = 0.0331 wR ₂ = 0.0806	R ₁ = 0.029 wR ₂ = 0.081	R ₁ = 0.0333 wR ₂ = 0.0892
Tot.,uniqu.data, R(int)	1927, 948, -	5895, 1893, 0.020	5583, 1996, 0.022	11 142, 2127, 0.015	19287, 2029, 0.310
N_{ref}, N_{par}	-	1893, 136	1996, 151	2127, 133	2029, 139
S	-	1.00	1.038	1.00	1.047
Max. and av. Shift/error	-	-	0.000, 0.000	-	0.000, 0.000
Min. and max. resd. dens	-	-0.10, 0.10	-0.198, 0.123	-0.17, 0.13	-0.269, 0.249

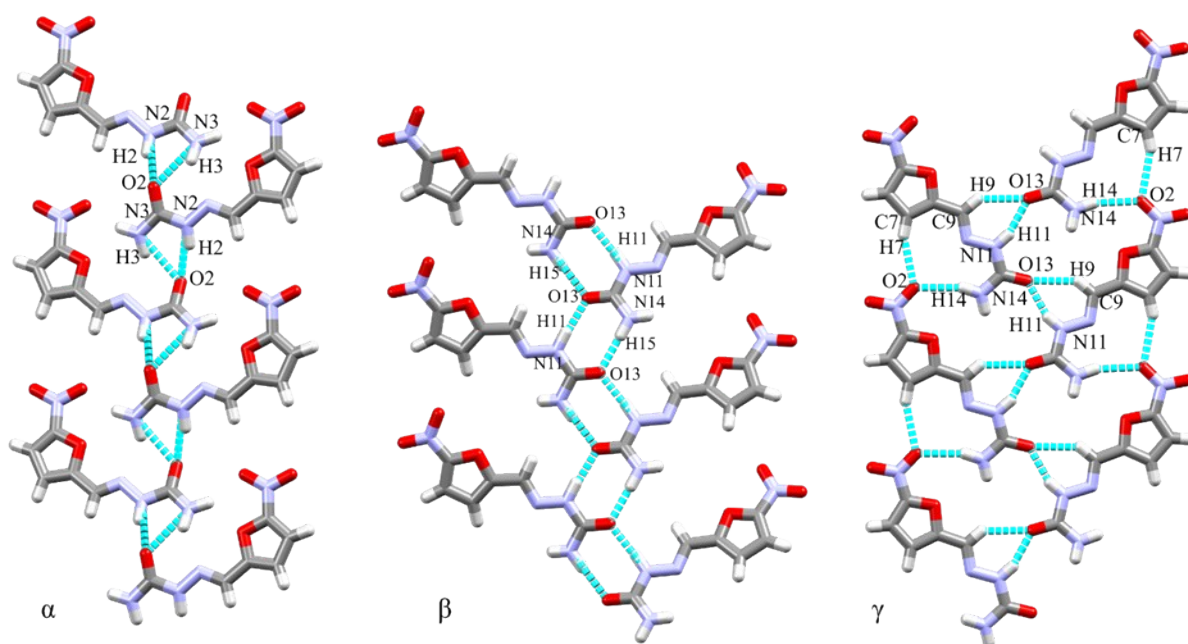


Figure S1. Hydrogen bonds between the NFZ molecules in the 3 reported polymorphs.

Table S3. List of acid solvents used and their respective crystallizations.

Solvents used	pKa	Results
HClO ₄ (dil)	≈ -10	co-crystal salt ¹
HClO ₄ (conc)	≈ -10	co-crystal salt ¹
H ₃ PO ₄ (dil)	2.12	solvate
H ₃ PO ₄ (conc)	2.12	solvate
H ₂ SO ₃ (dil)	1.81	β-polymorph
H ₂ SO ₃ (conc)	1.81	β-polymorph
HNO ₃ (dil)	< 1	β-polymorph
HNO ₃ (conc)	< 1	β-polymorph

Table S4. Crystallographic data of the three multicomponent crystals of NFZ.

	4NFZ•[H₃O⁺][ClO₄⁻]	NFZ•H₃PO₄	NFZ•PA
Molecular formula	C ₆ H ₆ N ₄ O ₄	C ₆ H ₉ N ₄ PO ₈	C ₉ H ₁₂ N ₄ O ₆
Formula weight	911.04	296.13	272.22
Temperature (K)	173(2)	173(2)	173(2)
Crystal system	Triclinic	Triclinic	Monoclinic
Space group	$P\bar{1}$	$P\bar{1}$	$P2_1/c$
a/Å	7.9863(16)	4.4913(9)	15.801(3)
b/Å	14.566(3)	10.893(2)	12.931(3)
c/Å	16.208(3)	12.672(3)	24.475(5)
α/°	77.88(3)	106.87(3)	90
β/°	80.90(3)	99.66(3)	90.04(3)
γ/°	87.87(3)	92.30(3)	90
Vol. /Å³	1820.2(7)	582.271	5000.8(17)
Z	2	2	16
MP /°C	223	221	241-248
ρ (gcm⁻³)	0.22	0.22	1.446
μ (mm⁻¹)	1.662	1.662	0.123
Dataset (hkl)	-16,16;-10,10;-10,10	-16,16;-10,10;-10,10	-21,21;-17,17;-32,32
F(000)	936.00	304.00	2272.00
Crystal size (mm)	0.07×0.11×0.13	0.29×0.39×0.56	0.12×0.13×0.15
Temperature (K)	173.15	173.15	173.15
Radiation [Å]	MoKα,	MoKα, 0.71073	MoKα, 0.71073
Theta min-max[°]	1.300/25.073	1.710/28.423	28.423
Final R indices [I>2.0 (I)]	R ₁ = 0.0527 wR ₂ = 0.1408	R ₁ = 0.0298 wR ₂ = 0.0812	R ₁ = 0.0473 wR ₂ = 0.1265
Tot., uniq.data, R(int)	3976, 6451, 0.0456	13757, 2900, 0.0337	7474, 12422, 0.0802
N_{ref}, N_{par}	6472, 619	2906, 196	12444, 705
S	0.964	1.036	1.009
Max. and av. Shift/error	0.000/0.000	0.000/0.000	0.000/0.011
Min. and max. resd. dens	-0.442, 0.511	-0.317, 0.345	-0.442, 0.511

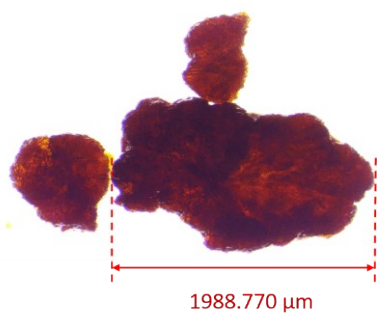


Figure S2. Photograph of uncut $4\text{NFZ}\cdot[\text{H}_3\text{O}^+][\text{ClO}_4^-]$ co-crystal salt.

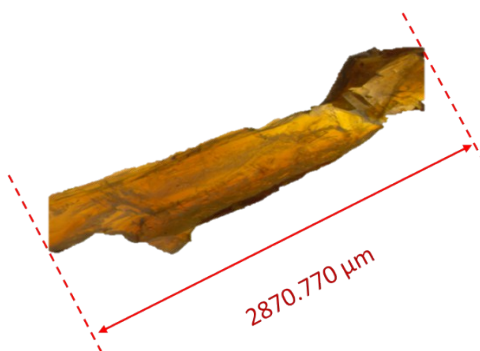


Figure S3. An uncut crystal of $\text{NFZ}\cdot\text{H}_3\text{PO}_4$.

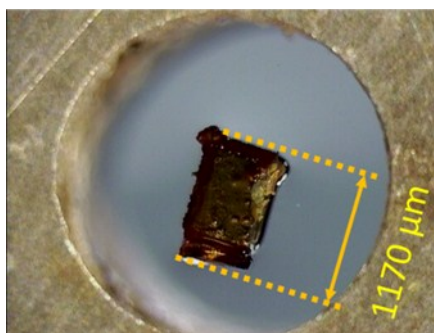


Figure S4. An uncut crystal of $\text{NFZ}\cdot\text{PA}$.

Table S5. The geometric parameters for intermolecular interactions in 4NFZ•[H₃O⁺][ClO₄⁻].

D-H...A	D-H (Å)	H...A (Å)	D...A (Å)	D-H...A (°)	Symmetry operators
MOLECULE A					
C8A-H8A...Cl17	0.950	2.912	3.736	145.79	-x, -y, -z +1
C8A-H8A...O20	0.950	2.566	3.455	155.91	-x, -y, -z +1
C9A-H9A...O19	0.950	2.465	3.107	124.84	
N11A-H11A...O2C	0.840	2.203	2.991	156.35	-1+x, -1+y, z
N14A-H14A...O3B	0.829	2.472	3.211	149.11	-1+x, y, z+1
N14A-H15A...O13D	0.841	2.164	2.995	169.77	
MOLECULE B					
C7B-H7B...O3C	0.950	2.501	3.426	164.41	-1+x, -1+y, z
C8B-H8B...O18	0.950	2.416	3.331	161.50	1-x, -y, -z
N11B-H11B...O2D	0.853	2.118	2.960	169.14	1+x, y, -1+z
N14B-H14B...O3C	0.877	2.357	3.190	158.68	-1+x, -1+y, z
N14B-H15B...O13A	0.828	2.095	2.915	170.81	
MOLECULE C					
C7C-H7C...O3D	0.950	2.548	3.458	160.48	1+x, y, -1+z
C8C-H8C...O21	0.950	2.479	3.217	134.53	2-x, 1-y, -z
N11C-H11C...O2A	0.829	2.412	3.063	135.92	-1+x, -1+y, z
N11C-H11C...O20	0.829	2.244	2.982	148.30	x, y+1, z
N14C-H14C...O2D	0.919	2.567	3.026	111.45	1+x, y, -1+z
N14C-H14C...O3D	0.919	2.272	3.167	164.10	1+x, y, -1+z
N14C-H14C...O13B	0.851	2.090	2.925	166.67	
MOLECULE D					
C8D-H8D...Cl17	0.950	2.942	3.697	137.36	1-x, 1-y, 1-z
C8D-H8D...O19	0.950	2.618	3.131	114.24	1-x, 1-y, 1-z
C8D-H8D...O21	0.950	2.580	3.509	166.14	1-x, 1-y, 1-z
N11D-H11D...O2B	0.877	2.095	2.958	167.98	-1+x, y, z+1
N14D-H14D...O3A	0.943	2.131	3.013	155.27	1+x, 1+y, z
N14D-H15D...O13C	0.802	2.224	3.024	175.06	
O16-H16A...O13A	0.900	1.969	2.772	147.66	
O16-H16B...O13C	0.902	1.591	2.439	155.05	
O16-H16C...O13D	0.905	1.613	2.508	169.33	

Table S6. The geometric parameters for intermolecular interactions in NFZ•H₃PO₄.

D-H...A	d(D-H) (Å)	d(H...A) (Å)	d(D...A) (Å)	<D-H...A(°)	Symmetry operators
C7-H7...O20	0.950	2.592	3.503	160.90	1-x, 1-y, 1-z
C8-H8...O20	0.950	2.477	3.360	154.62	-1+x, y, 1+z
C9-H9...O18	0.950	2.587	3.520	167.21	2-x, 1-y, 1-z
N11-H11...O13	0.881	1.983	2.862	175.91	2-x, 1-y, 1-z
N14-H15...O19	0.877	2.305	3.162	165.47	
N14-H14...O2	0.840	2.300	3.029	145.18	-x, -y, 1-z
O18-H18...O13	0.827	1.687	2.501	167.79	
O19-H19...O17	0.826	1.740	2.566	178.85	2-x, -y, -z
O20-H20...O17	0.774	1.797	2.568	174.96	-1+x, y, z

Table S7. Hydrogen bonds in NFZ•PA.

D-H...A	d(D-H) (Å)	d(H...A) (Å)	d(D...A) (Å)	<D-H...A (°)	Symmetry operators
C8A-H8A...O15D	0.950	2.507	3.451	172.63	-1+x, y, z
N11A-H11A...O17A	0.915	1.867	2.779	174.42	
O15A-H15A...O13A	0.959	1.690	2.641	170.38	
N14A-H14A...O3C	0.893	2.227	2.897	131.44	
N14A-H14B...O13B	0.864	2.020	2.883	176.88	
C8B-H8B...O15C	0.950	2.446	3.393	174.64	x, y, 1+z
N11B-H11B...O17B	0.950	1.836	2.783	173.96	
N14B-H14C...O3D	0.891	2.255	2.914	130.54	-1+x, y, 1+z
N14B-H14D...O13A	0.855	2.062	2.915	175.29	
O15B-H15B...O13B	0.948	1.705	2.643	169.69	
C7C-H7C...O2A	0.950	2.516	3.457	170.72	1+x, y, z
C8C-H8C...O15B	0.950	2.450	3.398	174.99	
N11C-H11C...O17C	0.941	1.859	2.798	174.88	
N14B-H14E...O3A	0.899	2.250	2.922	131.20	1+x, y, z
N14C-H14F...O13D	0.898	2.001	2.897	176.16	
C7D-H7D...O2B	0.950	2.531	3.466	168.07	x, y, -1+z
C8D-H8D...O15A	0.950	2.461	3.411	177.48	1+x, y, -1+z
N11D-H11D...O17D	0.934	1.857	2.790	175.67	
N14D-H14G...O13C	0.893	2.016	2.908	177.27	
N14D-H14H...O3B	0.894	2.205	2.903	134.60	x, y, -1+z
O15D-H15D...O13D	1.002	1.654	2.645	169.01	

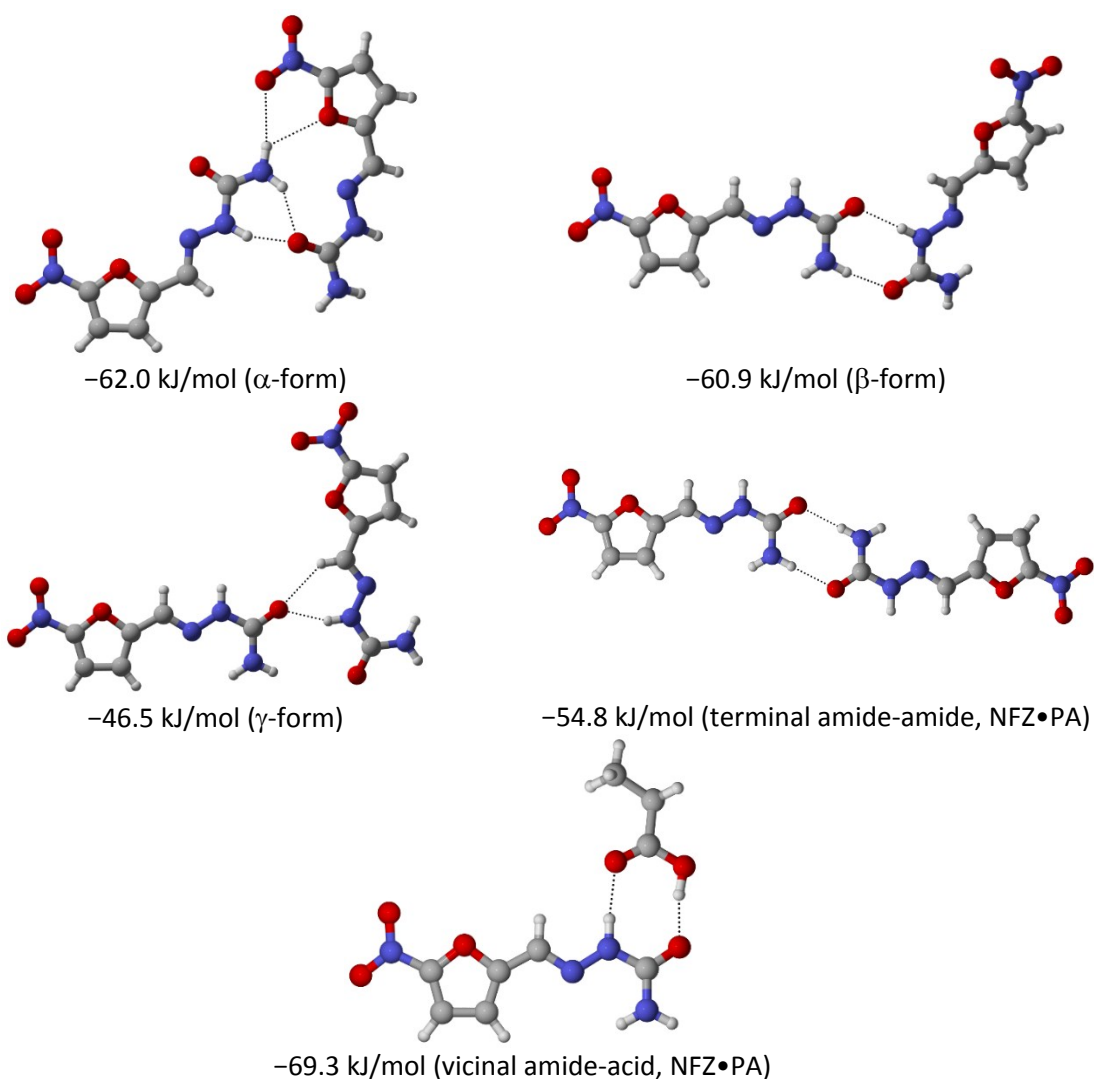


Figure S5. Interaction energies of fragments taken from the crystal structure and used without further optimization. Calculations done at the DSD-PBEP86/def2-QZVPP level of theory, corrected for BSSE using the counterpoise procedure.

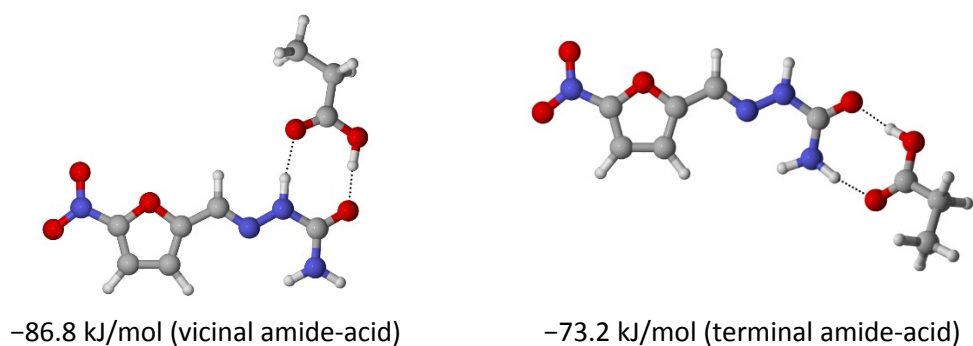


Figure S6. Interaction energies of possible amide-PA synthons after geometry optimization. Calculations done at the DSD-PBEP86/def2-QZVPP//PBE0-D3(BJ)/def2-TZVP level of theory, corrected for BSSE using the counterpoise procedure.

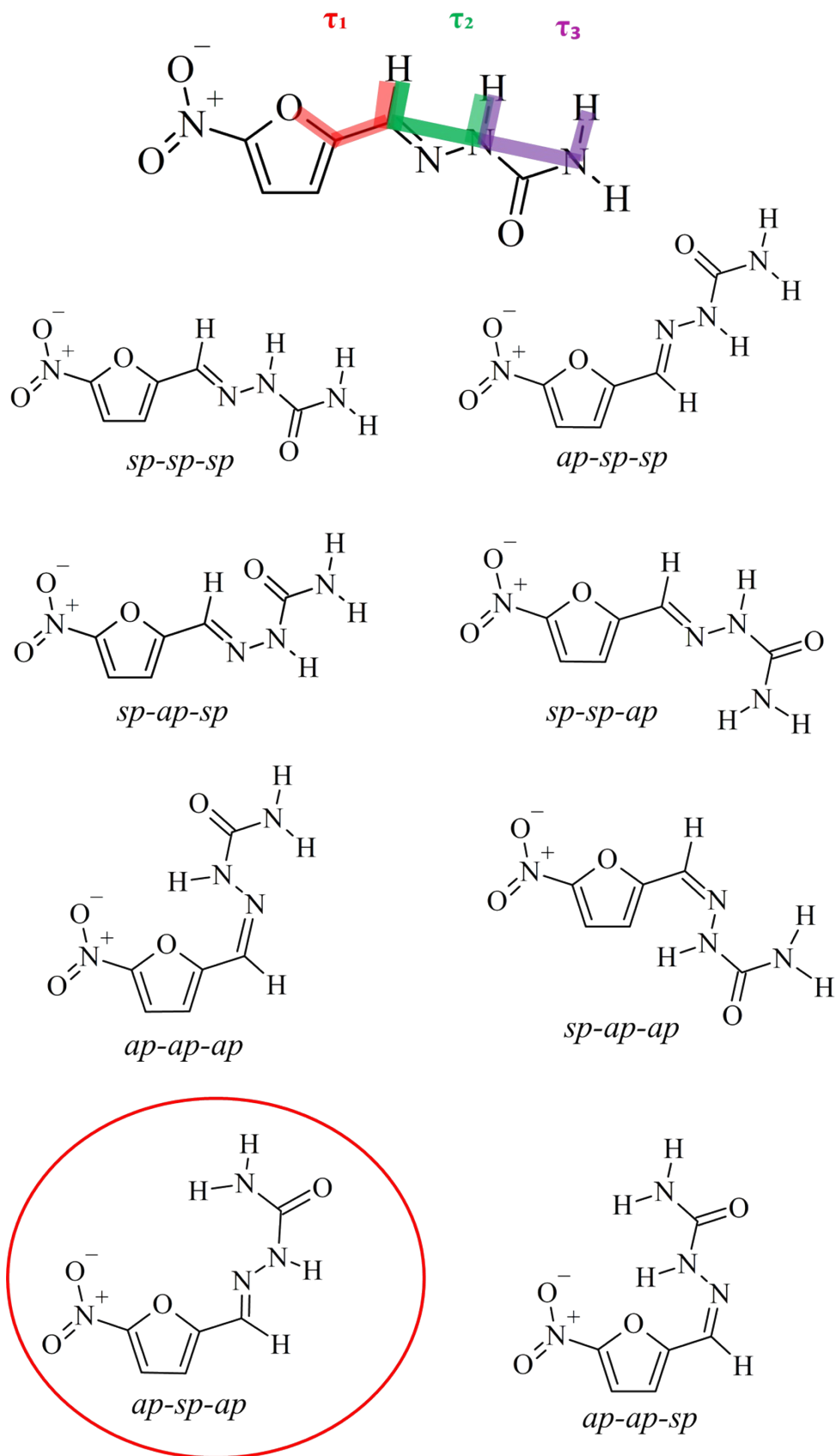
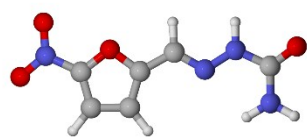
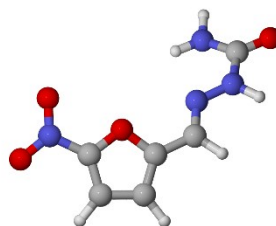


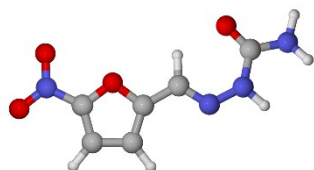
Figure S7 Eight possible conformers arising from the *sp* and *ap* torsion combinations. Newly found conformer of NFZ in NFZ•H₃PO₄ crystal is circled in red.



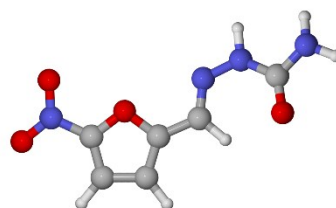
sp-sp-ap
0.0 kJ/mol



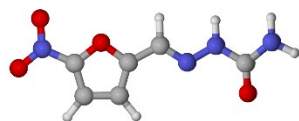
ap-sp-ap*new
+6.0 kJ/mol



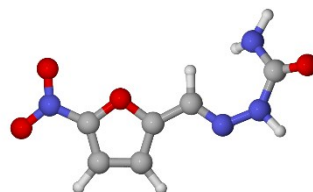
sp-ap-sp
+20.4 kJ/mol



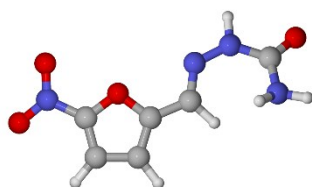
ap-ap-sp
+21.8 kJ/mol



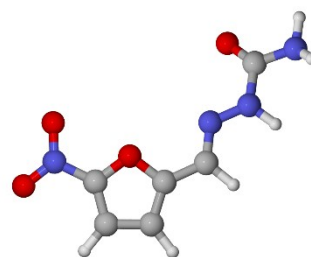
sp-sp-sp
+28.7 kJ/mol



sp-ap-ap
+33.1 kJ/mol



ap-ap-ap
+37.7 kJ/mol



ap-sp-sp
+38.1 kJ/mol

Figure S8. Relative conformational energies, calculated at the DSD-PBEP86/def2-QZVPP//PBE0-D3(BJ)/def2-TZVP level of theory.

Table S8. Torsion angles of NFZ in polymorphs α , β and γ and in MCCs.

	τ_1 (O5-C6-C9-H9)	τ_2 (H9-C9...N11-H11)	τ_3 (H11-N11...N14-H14)	conformer class
α-polymorph*	177.46	-10.14	-1.32	<i>ap-sp-sp</i>
β-polymorph	-3.07	-8.54	-162.67	<i>sp-sp-ap</i>
γ-polymorph	-0.71	3.29	174.22	<i>sp-sp-ap</i>
4NFZ•[H₃O⁺][ClO₄⁻]				
molecule A	6.57	-0.92	-169.95	<i>sp-sp-ap</i>
molecule B	2.15	2.54	171.58	<i>sp-sp-ap</i>
molecule C	0.53	4.29	168.71	<i>sp-sp-ap</i>
molecule D	-1.20	-1.46	-174.73	<i>sp-sp-ap</i>
NFZ•H₃PO₄	176.04	5.47	168.72	<i>ap-sp-ap</i>
NFZ•PA				
molecule A	-1.96	0.36	174.03	<i>sp-sp-ap</i>
molecule B	-3.26	-5.99	-172.71	<i>sp-sp-ap</i>
molecule C	-3.08	-1.36	178.24	<i>sp-sp-ap</i>
molecule D	0.43	2.82	175.03	<i>sp-sp-ap</i>

* structural data of α was retrieved from Mercury, hence the different atomic numbering.

Table S9. Relevant torsion angles and their resulting conformation (continued to next pages).

Refcode	Sp. Grp	Fragment	τ_1	τ_2	τ_3	Class
BZALSC01	$P2_1/c$	1	6.118	-8.06	2.229	<i>sp-sp-ap</i>
BZALSC01	$P2_1/c$	2	-175.454	-8.06	2.229	<i>ap-sp-sp</i>
BZALSC10	$P2_1/c$	1	5.522	3.659	158.158	<i>sp-sp-ap</i>
BZALSC10	$P2_1/c$	2	-176.56	3.659	158.158	<i>ap-sp-ap</i>
DODGEI	$P1_12_1/b$	1	-174.576	10.501	-19.229	<i>sp-sp-sp</i>
DODGEI	$P1_12_1/b$	2	5.314	10.501	-19.229	<i>sp-sp-sp</i>
DUMZAN	$P3_12_1$	1	-161.039	1.066	179.26	<i>sp-sp-ap</i>
DUMZAN	$P3_12_1$	2	19.471	1.066	179.26	<i>sp-sp-ap</i>
EDELUV	$P\bar{1}$	1	178.111	-11.639	12.359	<i>sp-sp-ap</i>
EDELUV	$P\bar{1}$	2	-2.418	-11.639	12.359	<i>sp-sp-sp</i>
EKILOZ	$P2/c$	1	79.441	-0.479	-173.708	<i>sc-sp-ap</i>
EKILOZ	$P2/c$	2	-68.837	-4.61	177.848	<i>ac-sp-ap</i>
EKILOZ	$P2/c$	3	-38.775	-0.479	-173.708	<i>ac-sp-ap</i>
EKILOZ	$P2/c$	4	50.119	-4.61	177.848	<i>ac-sp-ap</i>
EKILOZ	$P2/c$	5	-159.138	-0.479	-173.708	<i>ap-sp-ap</i>
EKILOZ	$P2/c$	6	168.841	-4.61	177.848	<i>sp-sp-ap</i>
ETIXOU	$P2_1/c$	1	-167.888	-1.565	-157.461	<i>sp-sp-ap</i>
ETIXOU	$P2_1/c$	2	11.192	-1.565	-157.461	<i>sp-sp-ap</i>
EVERED	$Pca2_1$	1	174.938	2.954	-1.75	<i>sp-sp-ac</i>
EVERED	$Pca2_1$	2	-179.421	0.536	-156.631	<i>ap-sp-ap</i>
EVERED	$Pca2_1$	3	-3.061	2.954	-1.75	<i>sp-sp-sp</i>
EVERED	$Pca2_1$	4	-2.265	0.536	-156.631	<i>sp-sp-ap</i>
EVERED01	$Pca2_1$	1	173.773	-9.123	177.454	<i>sp-sp-ap</i>
EVERED01	$Pca2_1$	2	-178.212	6.637	-177.645	<i>ap-sp-ap</i>
EVERED01	$Pca2_1$	3	-4.528	-9.123	177.454	<i>sp-sp-ap</i>
EVERED01	$Pca2_1$	4	-1.546	6.637	-177.645	<i>sp-sp-ap</i>
EVERED02	$Pca2_1$	1	-179.093	15.305	-20.536	<i>ap-sp-sp</i>
EVERED02	$Pca2_1$	2	172.494	2.178	-5.335	<i>sp-sp-ap</i>
EVERED02	$Pca2_1$	3	-1.91	15.305	-20.536	<i>sp-sp-sp</i>
EVERED02	$Pca2_1$	4	-5.722	2.178	-5.335	<i>sp-sp-sp</i>
FUDQIE	$P2_1/a$	1	15.87	0.582	178.598	<i>sp-sp-ap</i>
FUDQIE	$P2_1/a$	2	-165.889	0.582	178.598	<i>ap-sp-ap</i>
FUNDUN	$P2_1/c$	1	-178.594	-5.04	-13.382	<i>ap-sp-sp</i>
FUNDUN	$P2_1/c$	2	-0.17	-5.04	-13.382	<i>sp-sp-sp</i>
GAQDOT	$P\bar{1}$	1	-178.596	0.256	-11.797	<i>sp-sp-ap</i>
GAQDOT	$P\bar{1}$	2	-177.773	-2.457	178.704	<i>ap-sp-ap</i>
GAQDOT	$P\bar{1}$	3	1.388	0.256	-11.797	<i>sp-sp-sp</i>
GAQDOT	$P\bar{1}$	4	1.86	-2.457	178.704	<i>sp-sp-ap</i>
GUHXOY	$C2/c$	1	-3.222	-2.536	-1.56	<i>sp-sp-ap</i>
GUHXOY	$C2/c$	2	178.24	-2.536	-1.56	<i>ap-sp-ap</i>
GUHXOY01	$I2/a$	1	3.941	-6.797	-177.933	<i>sp-sp-ap</i>
GUHXOY01	$I2/a$	2	-177.613	-6.797	-177.933	<i>ap-sp-ap</i>

GUHXOY02	I_2/a	1	3.941	-6.797	-177.933	<i>sp-sp-ap</i>
GUHXOY02	I_2/a	2	-177.613	-6.797	-177.933	<i>ap-sp-ap</i>
GUMNIN	$p\bar{1}$	1	4.482	0.12	-169.56	<i>sp-sp-ap</i>
GUMNIN	$p\bar{1}$	2	177.16	0.12	-169.56	<i>ap-sp-ap</i>
HAXHOG	P_{2_1}/c	1	4.121	8.294	-175.615	<i>sp-sp-ap</i>
HAXHOG	P_{2_1}/c	2	-172.783	8.294	-175.615	<i>ap-sp-ap</i>
IJOXAH	P_{2_1}/c	1	171.293	1.359	-11.426	<i>sp-sp-ap</i>
IJOXAH	P_{2_1}/c	2	-7.982	1.359	-11.426	<i>sp-sp-sp</i>
JOWSIZ	$p\bar{1}$	1	178.933	-2.49	176.911	<i>sp-sp-ap</i>
JOWSIZ	$p\bar{1}$	2	1.915	-2.49	176.911	<i>sp-sp-ap</i>
KEZKIK	$p\bar{1}$	1	1.116	-6.962	179.813	<i>sp-sp-ap</i>
KEZKIK	$p\bar{1}$	2	-176.177	-6.571	-174.642	<i>ap-sp-ap</i>
KEZKIK	$p\bar{1}$	3	-179.692	-6.962	179.813	<i>ap-sp-ap</i>
KEZKIK	$p\bar{1}$	4	2.135	-6.571	-174.642	<i>sp-sp-ap</i>
KUHGEA	P_{2_1}/n	1	-0.27	-2.171	-16.39	<i>sp-sp-ap</i>
KUHGEA	P_{2_1}/n	2	-179.452	-2.171	-16.39	<i>ap-sp-ap</i>
LATFER	P_{2_1}/c	1	-6.775	-4.786	17.934	<i>sp-sp-ap</i>
LATFER	P_{2_1}/c	2	172.694	-4.786	17.934	<i>ap-sp-ap</i>
LATFIV	P_{2_1}/a	1	-170.174	10.209	-11.973	<i>sp-sp-ap</i>
LATFIV	P_{2_1}/a	2	9.115	10.209	-11.973	<i>sp-sp-sp</i>
MOPBUP	P_{2_1}/c	1	-3.476	0.259	157.042	<i>sp-sp-ap</i>
MOPBUP	P_{2_1}/c	2	175.959	0.259	157.042	<i>ap-sp-ap</i>
MOPCAW	C_2/c	1	4.964	-14.261	-160.544	<i>sp-sp-ap</i>
MOPCAW	C_2/c	2	-175.603	-14.261	-160.544	<i>ap-sp-ap</i>
MUKXEV	$p\bar{1}$	1	-173.148	11.062	141.205	<i>sp-sp-ac</i>
MUKXEV	$p\bar{1}$	2	173.323	-8.644	10.708	<i>ap-sp-sp</i>
MUKXEV	$p\bar{1}$	3	174.42	-2.822	-11.844	<i>ap-sp-sp</i>
MUKXEV	$p\bar{1}$	4	-174.276	10.839	175.696	<i>ap-sp-ap</i>
MUKXEV	$p\bar{1}$	5	7.459	11.062	141.205	<i>sp-sp-sc</i>
MUKXEV	$p\bar{1}$	6	-7.977	-8.644	10.708	<i>sp-sp-sp</i>
MUKXEV	$p\bar{1}$	7	-2.954	-2.822	-11.844	<i>sp-sp-sp</i>
MUKXEV	$p\bar{1}$	8	3.209	10.839	175.696	<i>sp-sp-ap</i>
PAVZAP	C_2/c	1	148.354	-16.85	174.229	<i>sc-sp-ap</i>
PAVZAP	C_2/c	2	-31.214	-16.85	174.229	<i>ac-sp-ap</i>
PIWFUW	$P_{2_1}2_12_1$	1	-44.923	-7.808	-178.722	<i>sc-sp-ap</i>
PIWFUW	$P_{2_1}2_12_1$	2	-58.717	2.055	-176.522	<i>ac-sp-ap</i>
PIWFUW	$P_{2_1}2_12_1$	3	67.318	14.367	-177.636	<i>ac-sp-ap</i>
PIWFUW	$P_{2_1}2_12_1$	4	68.727	-7.808	-178.722	<i>ac-sp-ap</i>
PIWFUW	$P_{2_1}2_12_1$	5	53.717	2.055	-176.522	<i>ac-sp-ap</i>
PIWFUW	$P_{2_1}2_12_1$	6	-176.508	14.367	-177.636	<i>ap-sp-ap</i>
PIWFUW	$P_{2_1}2_12_1$	7	-164.592	-7.808	-178.722	<i>ap-sp-ap</i>
PIWFUW	$P_{2_1}2_12_1$	8	-172.964	2.055	-176.522	<i>ap-sp-ap</i>
PIWFUW	$P_{2_1}2_12_1$	9	-52.658	14.367	-177.636	<i>ac-sp-ap</i>
PIWFUW01	$P_{2_1}2_12_1$	1	-44.923	-7.808	-178.722	<i>sc-sp-ap</i>
PIWFUW01	$P_{2_1}2_12_1$	2	-58.717	2.055	-176.522	<i>ac-sp-ap</i>

PIWFUW01	$P_{2_1 2_1 2_1}$	3	67.318	14.367	-177.636	<i>ac-sp-ap</i>
PIWFUW01	$P_{2_1 2_1 2_1}$	4	68.727	-7.808	-178.722	<i>ac-sp-ap</i>
PIWFUW01	$P_{2_1 2_1 2_1}$	5	53.717	2.055	-176.522	<i>ac-sp-ap</i>
PIWFUW01	$P_{2_1 2_1 2_1}$	6	-176.508	14.367	-177.636	<i>ap-sp-ap</i>
PIWFUW01	$P_{2_1 2_1 2_1}$	7	-164.592	-7.808	-178.722	<i>ap-sp-ap</i>
PIWFUW01	$P_{2_1 2_1 2_1}$	8	-172.964	2.055	-176.522	<i>ap-sp-ap</i>
PIWFUW01	$P_{2_1 2_1 2_1}$	9	-52.658	14.367	-177.636	<i>ac-sp-ap</i>
TAKREC	$C_{2/c}$	1	175.352	-1.252	156.046	<i>sp-sp-ap</i>
TAKREC	$C_{2/c}$	2	-4.172	-1.252	156.046	<i>sp-sp-ap</i>
TAKREC01	$p\bar{1}$	1	-175.305	-5.559	-152.45	<i>ap-sp-ap</i>
TAKREC01	$p\bar{1}$	2	-178.219	-9.865	55.036	<i>ap-sp-ac</i>
TAKREC01	$p\bar{1}$	3	3.319	-5.559	-152.45	<i>sp-sp-ap</i>
TAKREC01	$p\bar{1}$	4	2.408	-9.865	55.036	<i>sp-sp-ac</i>
TAKREC02	$C_{2/c}$	1	176.78	7.599	147.232	<i>sp-sp-ac</i>
TAKREC02	$C_{2/c}$	2	-2.84	7.599	147.232	<i>sp-sp-ap</i>
TIVGOU	$p\bar{1}$	1	-179.314	0.077	-174.008	<i>sp-sp-ap</i>
TIVGOU	$p\bar{1}$	2	177.714	0.988	179.364	<i>sp-sp-ap</i>
TIVGOU	$p\bar{1}$	3	0.61	0.077	-174.008	<i>sp-sp-ap</i>
TIVGOU	$p\bar{1}$	4	15.858	0.988	179.364	<i>sp-sp-ap</i>
TUBQOW	$P_{2_1/a}$	1	171.214	3.48	30.25	<i>sp-sp-ap</i>
TUBQOW	$P_{2_1/a}$	2	-9.409	3.48	30.25	<i>sp-sp-ac</i>
TUBQUC	$P_{2_1/c}$	1	-0.034	-15.672	-6.667	<i>sp-sp-ap</i>
TUBQUC	$P_{2_1/c}$	2	178.169	-15.672	-6.667	<i>ap-sp-sp</i>
TUBRAJ	$P_{2_1/a}$	1	17.064	0.196	-21.094	<i>sp-sp-sp</i>
TUBRAJ	$P_{2_1/a}$	2	-163.247	0.196	-21.094	<i>ap-sp-sp</i>
TUBREN	$P_{2_1/a}$	1	-19.183	-1.369	171.284	<i>sp-sp-ap</i>
TUBREN	$P_{2_1/a}$	2	161.321	-1.369	171.284	<i>ap-sp-ap</i>
UMAKIE	$P_{2_1/a}$	1	167.294	-9.182	171.851	<i>sp-sp-ap</i>
UMAKIE	$P_{2_1/a}$	2	-10.22	-9.182	171.851	<i>sp-sp-ap</i>
UWIREZ	P_{2_1}	1	68.15	5.427	-179.892	<i>sc-sp-ap</i>
UWIREZ	P_{2_1}	2	-38.889	5.427	-179.892	<i>ac-sp-ap</i>
UWIREZ	P_{2_1}	3	-165.133	5.427	-179.892	<i>ap-sp-ap</i>
VILPIQ	P_{2_1}	1	-154.655	3.763	179.273	<i>ap-sp-ap</i>
VILPIQ	P_{2_1}	2	79.28	3.763	179.273	<i>sp-sp-ap</i>
VILPIQ	P_{2_1}	3	-36.123	3.763	179.273	<i>ac-sp-ap</i>
VORKET	$P_{2_1/c}$	1	-9.662	-11.179	166.634	<i>sp-sp-ap</i>
VORKET	$P_{2_1/c}$	2	167.886	-11.179	166.634	<i>ap-sp-ap</i>
VORKET01	$P_{2_1/c}$	1	9.807	11.536	-167.326	<i>sp-sp-ap</i>
VORKET01	$P_{2_1/c}$	2	-167.896	11.536	-167.326	<i>ap-sp-ap</i>
WERVEU	$P_{2_1/a}$	1	177.457	-10.14	-161.818	<i>ap-sp-ap</i>
WERVEU	$P_{2_1/a}$	2	-2.758	-10.14	-161.818	<i>sp-sp-ap</i>
WERVEU01	P_{2_1}	1	5.348	8.586	-15.69	<i>sp-sp-sp</i>
WERVEU01	P_{2_1}	2	-174.361	8.586	-15.69	<i>ap-sp-sp</i>
WERVEU02	$P_{2_1/c}$	1	-1.062	1.433	-1.715	<i>sp-sp-sp</i>
WERVEU02	$P_{2_1/c}$	2	-178.363	1.433	-1.715	<i>ap-sp-sp</i>

WIGPAF	$p\bar{1}$	1	-173.108	2.113	-149.444	<i>sp-sp-ac</i>
WIGPAF	$p\bar{1}$	2	3.762	2.113	-149.444	<i>sp-sp-sc</i>
XAXXUQ	$p\bar{1}$	1	2.41	-4.566	-2.412	<i>sp-sp-ap</i>
XAXXUQ	$p\bar{1}$	2	-177.954	-4.566	-2.412	<i>ap-sp-sp</i>
XUTVIT	$P2_1/c$	1	-2.238	7.128	-7.986	<i>sp-sp-ap</i>
XUTVIT	$P2_1/c$	2	177.185	7.128	-7.986	<i>ap-sp-sp</i>
XUTVOZ	$p\bar{1}$	1	176.836	-1.509	14.429	<i>ap-sp-sp</i>
XUTVOZ	$p\bar{1}$	2	-3.642	-1.509	14.429	<i>sp-sp-sp</i>
YAGFIX	$P2_1/c$	1	7.33	-1.108	-151.271	<i>sp-sp-ap</i>
YAGFIX	$P2_1/c$	2	-171.318	-1.108	-151.271	<i>ap-sp-ap</i>
YAVVAU	$P2/c$	1	177.36	-10.513	9.118	<i>ap-sp-sp</i>
YAVVAU	$P2/c$	2	-0.888	-10.513	9.118	<i>sp-sp-sp</i>
YFGBIB	$P2_1/c$	1	178.206	0.67	-176.513	<i>sp-sp-ap</i>
YFGBIB	$P2_1/c$	2	-167.313	8.543	172.502	<i>ap-sp-ap</i>
YFGBIB	$P2_1/c$	3	-5.149	0.67	-176.513	<i>sp-sp-ap</i>
YFGBIB	$P2_1/c$	4	15.651	8.543	172.502	<i>sp-sp-ap</i>
YFGBIB	$P2_1/c$	5	-4.926	-3.046	-174.28	<i>sp-sp-ap</i>
YFGBIB	$P2_1/c$	6	0.9	5.258	175.78	<i>sp-sp-ap</i>
YFGBIB	$P2_1/c$	7	174.036	-3.046	-174.28	<i>ap-sp-ap</i>
YFGBIB	$P2_1/c$	8	-176.533	5.258	175.78	<i>ap-sp-ap</i>
YFGBOH	$P2_1/c$	1	2.319	7.451	154.868	<i>sp-sp-ap</i>
YFGBOH	$P2_1/c$	2	-179.966	7.451	154.868	<i>sp-sp-ap</i>
YIFTOX	$P2_1/c$	1	174.711	-0.628	-160.651	<i>sp-sp-ap</i>
YIFTOX	$P2_1/c$	2	-6.993	-0.628	-160.651	<i>sp-sp-ap</i>
YIFVUF	$P2_1/c$	1	-4.018	1.662	-166.483	<i>sp-sp-ap</i>
YIFVUF	$P2_1/c$	2	178.319	1.662	-166.483	<i>ap-sp-ap</i>
YOYNOP	$P2_1/a$	1	9.941	-2.714	42.537	<i>sp-sp-ac</i>
YOYNOP	$P2_1/a$	2	-167.953	-2.714	42.537	<i>ap-sp-ac</i>
YOYNOP01	$P2_1/c$	1	10.524	4.262	-169.823	<i>sp-sp-ap</i>
YOYNOP01	$P2_1/c$	2	-168.574	4.262	-169.823	<i>ap-sp-ap</i>
ZAMZUI	$P2_1/n$	1	178.179	-2.12	-170.134	<i>ap-sp-ap</i>
ZAMZUI	$P2_1/n$	2	-1.215	-2.12	-170.134	<i>sp-sp-sp</i>
ZINZIH	$p\bar{1}$	1	178.501	2.646	169.21	<i>sp-sp-sp</i>
ZINZIH	$p\bar{1}$	2	-2.616	2.646	169.21	<i>sp-sp-ap</i>

Powder X-ray diffraction of multicomponent crystals of NFZ

The PXRD pattern of the co-crystal salt was recorded and compared to the generated powder pattern of $4\text{NFZ}\cdot[\text{H}_3\text{O}^+][\text{ClO}_4^-]$ (green in Figure S9). The scarcity of the crystals and the poor crystallinity of the material resulted in signal poor PXRD patterns. The generated pattern is representative of the bulk of the solvent based crystallization (bulk pattern is blue in Figure S9). The generated pattern was also compared to the pattern of the material obtained from a 45 minute long liquid assisted grinding (LAG) to show that the $4\text{NFZ}\cdot[\text{H}_3\text{O}^+][\text{ClO}_4^-]$ co-crystal salt can be prepared using mechanochemical methods.

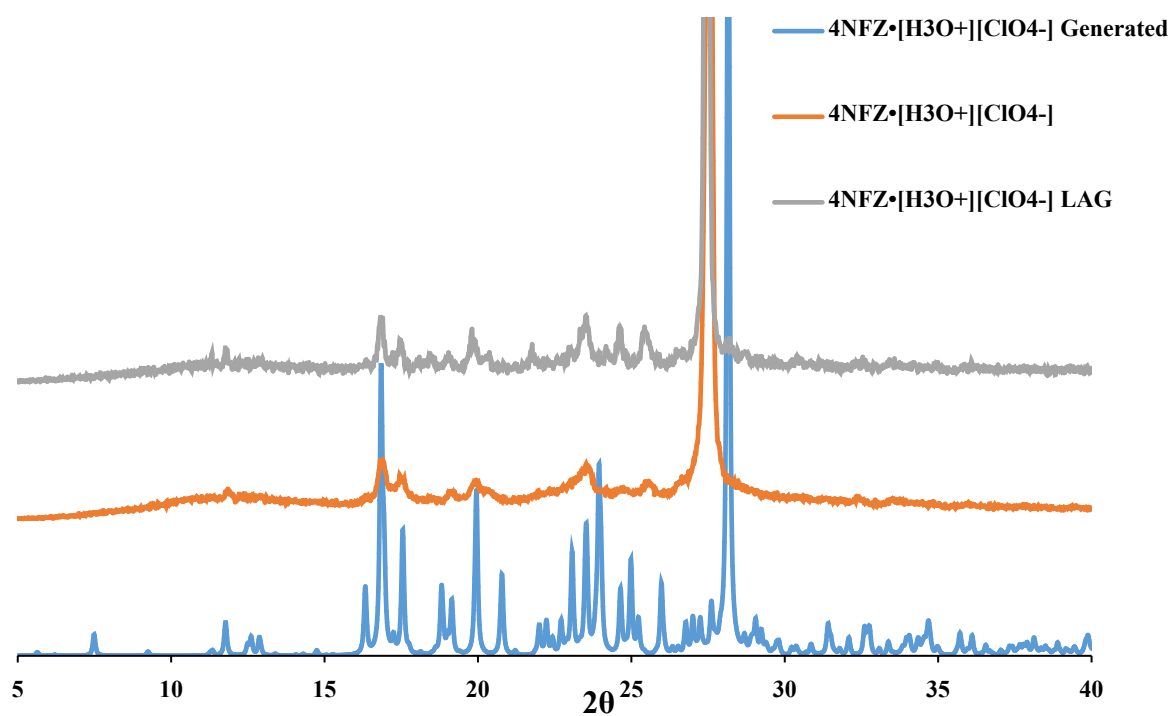


Figure S9. PXRD patterns of the samples prepared with different methods of $4\text{NFZ}\cdot[\text{H}_3\text{O}^+][\text{ClO}_4^-]$.

The PXRD patterns of the $\text{NFZ}\cdot\text{H}_3\text{PO}_4$ solvate were much more intense and this made the comparison easier. The bulk material was representative of the selected single crystal and also the 45 mins LAG were successful to reproduce the multicomponent crystal. The LAG did not yield 100% product and some remaining peaks from the starting materials can be seen on the pattern (Figure S10). The crystallisation of NFZ with PA yielded very few crystals, thus the PXRD pattern of the bulk crystals are signal poor. The generated pattern from the single crystal, the bulk and the 45 mins LAG of $\text{NFZ}\cdot\text{PA}$ are represented as green, blue and red, respectively on Figure S11.

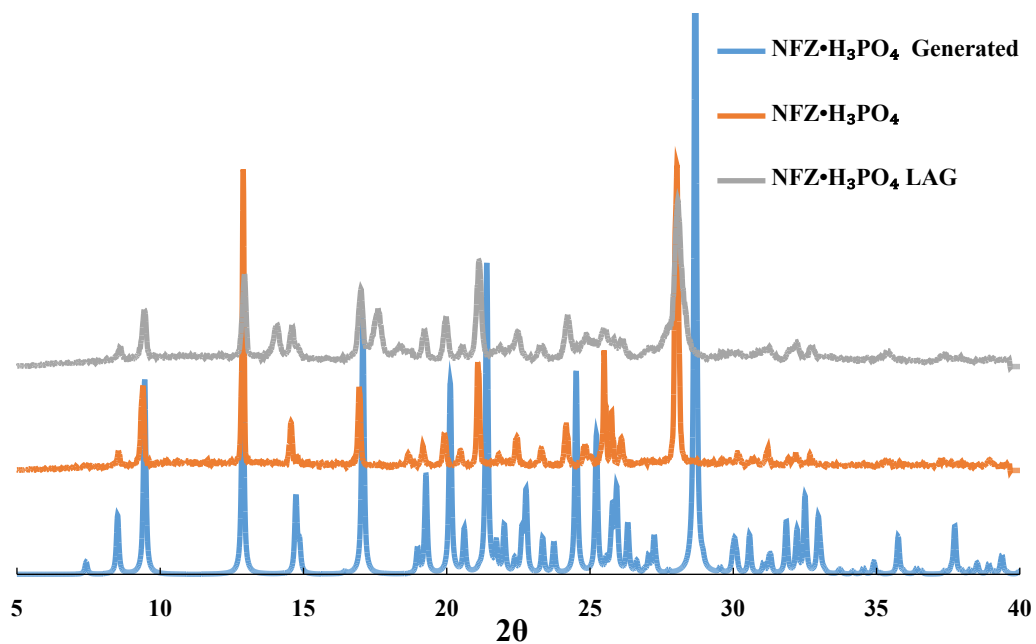


Figure S10. PXRD patterns of the samples prepared with different methods of $\text{NFZ}\cdot\text{H}_3\text{PO}_4$.

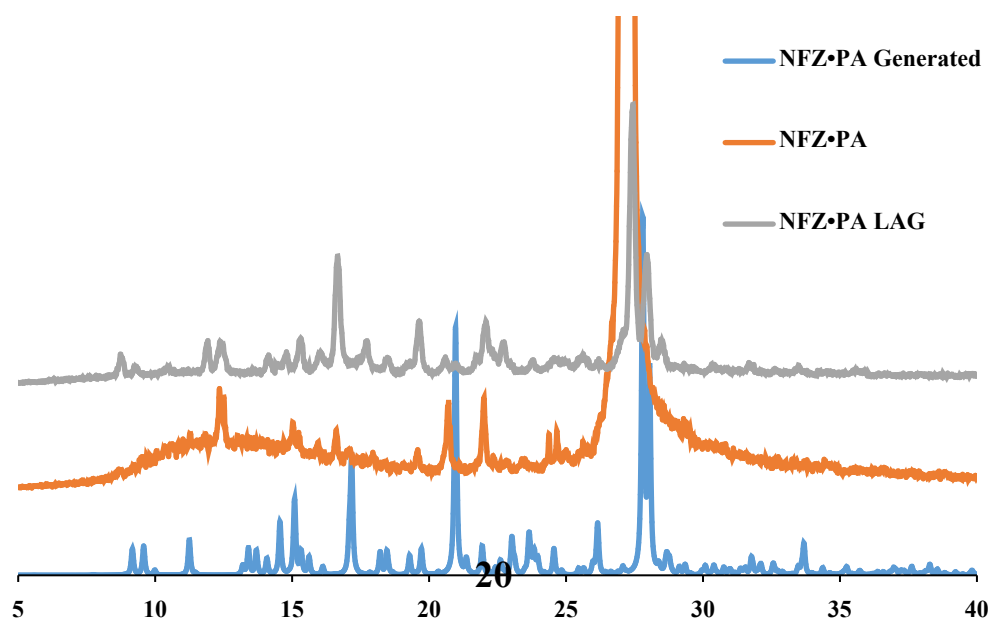


Figure S11. PXRD patterns of the samples prepared with different methods of $\text{NFZ}\cdot\text{PA}$.

Thermal analysis of multicomponent crystals of NFZ

Figure S12 shows the melting profile of $4\text{NFZ}\cdot[\text{H}_3\text{O}^+][\text{ClO}_4^-]$ crystals (green) with two thermal events ($T_{\text{onset1}} = 182.07^\circ\text{C}$ and $T_{\text{peak1}} = 188.65^\circ\text{C}$; $T_{\text{onset2}} = 223.59^\circ\text{C}$ and $T_{\text{peak2}} = 237.74^\circ\text{C}$). The DSC curve of the compound obtained with LAG (blue) has two similar thermal events ($T_{\text{onset1}} = 174.80^\circ\text{C}$ and $T_{\text{peak1}} = 180.83^\circ\text{C}$; $T_{\text{onset2}} = 219.32^\circ\text{C}$ and $T_{\text{peak2}} = 236.99^\circ\text{C}$). The first endotherm may be related to the desolvation of the co-crystal salt and the second endotherm is most likely related to the melting of the NFZ. This theory is supported well by the TGA results (Figure S13). The curve shows a gradual mass loss via a three-step transformation. The first mass loss step (calculated at 12.9 %) corresponds to the theoretical value of 13.0 % that is related to the desolvation and losing the $[\text{H}_3\text{O}^+][\text{ClO}_4^-]$ moieties. This is followed by a complex thermal decomposition.

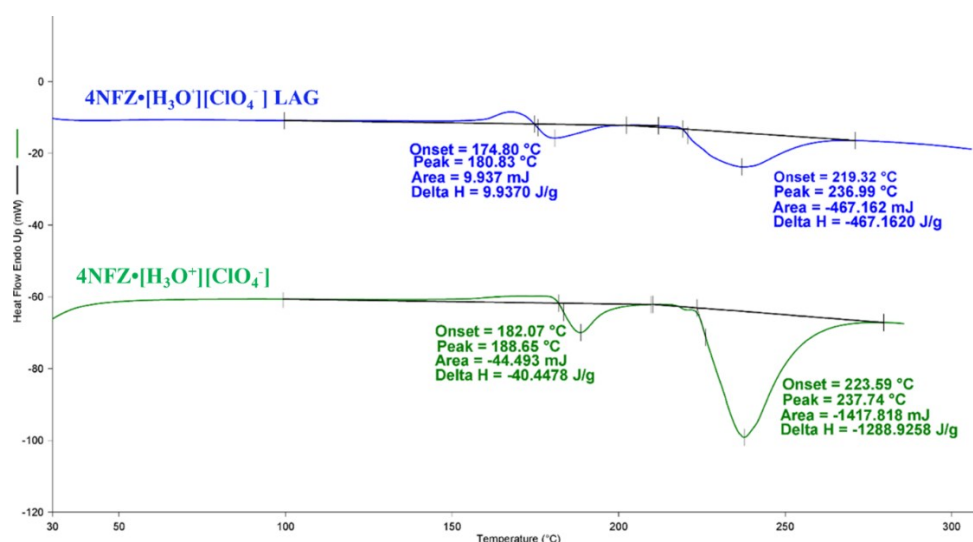


Figure S12. DSC curves of $4\text{NFZ}\cdot[\text{H}_3\text{O}^+][\text{ClO}_4^-]$ bulk material and samples obtained from LAG.

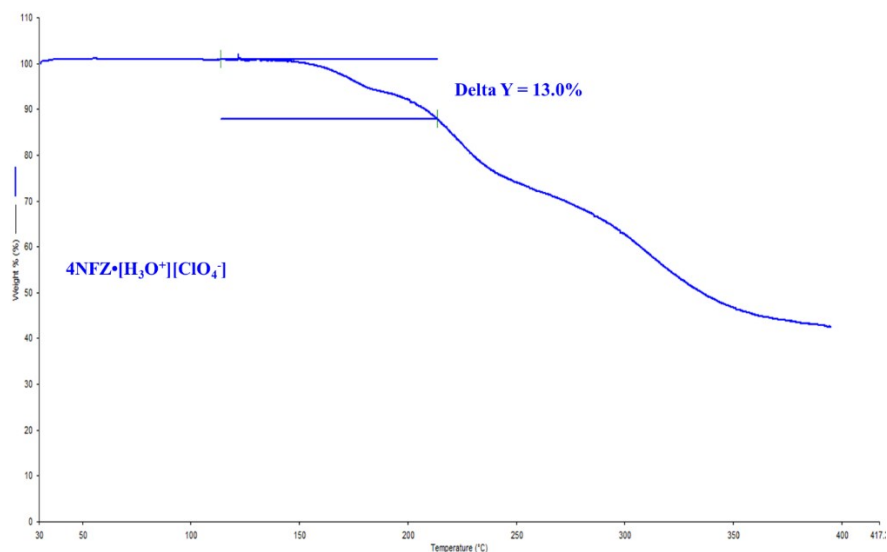


Figure S13. Thermal analysis curve showing steps of mass loss of $4\text{NFZ}\cdot[\text{H}_3\text{O}^+][\text{ClO}_4^-]$.

Crystals of $\text{NFZ}\cdot\text{H}_3\text{PO}_4$ were obtained from some of the performed experiments and their thermal behaviour were recorded with DSC (Figure S14). Similar to the DSC of the $4\text{NFZ}\cdot[\text{H}_3\text{O}^+][\text{ClO}_4^-]$ crystals, two thermal events are observed ($T_{\text{onset1}} = 179.44^\circ\text{C}$ and $T_{\text{peak1}} = 186.83^\circ\text{C}$; $T_{\text{onset2}} = 222.73^\circ\text{C}$ and $T_{\text{peak2}} = 241.7^\circ\text{C}$). The analysis of the material obtained via LAG shows similar behaviour to the bulk material of $\text{NFZ}\cdot\text{H}_3\text{PO}_4$ and support that the compound can also be synthesized via grinding ($T_{\text{onset1}} = 179.97^\circ\text{C}$ and $T_{\text{peak1}} = 187.78^\circ\text{C}$; $T_{\text{onset2}} = 232.21^\circ\text{C}$ and $T_{\text{peak2}} = 244.28^\circ\text{C}$). The TGA result reveals a complex, multi-step decomposition process (Figure S15). The rough estimate of the overall mass loss in the initial phase is 32 % and this corresponds well to the loss of the H_3PO_4 moiety.

The DSC and the TGA curves of $\text{NFZ}\cdot\text{PA}$ are shown on Figure S16. (These data were collected on a TA instrument with a heating rate of $10^\circ\text{C}/\text{min}$.) The DSC curve shows two thermal events, where the first one ($T_{\text{onset}} = 80.48^\circ\text{C}$ and $T_{\text{peak}} = 87.22^\circ\text{C}$) is related to the desolvation of the $\text{NFZ}\cdot\text{PA}$ crystals, while the second endotherm ($T_{\text{onset}} = 240.60$ and $T_{\text{peak}} = 244.38$) can be associated to the melting on the NFZ. The TGA results support the desolvation process; the 26.21 % mass loss agrees well with the loss of the PA moiety.

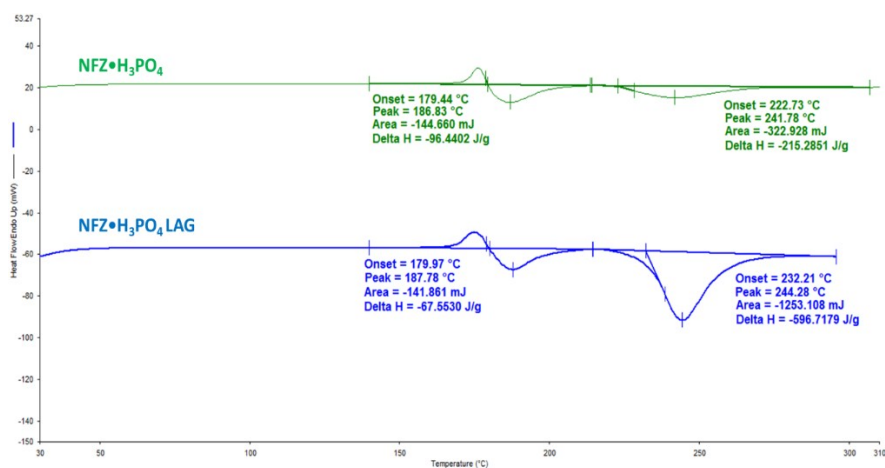


Figure S14. DSC curve of $\text{NFZ}\cdot\text{H}_3\text{PO}_4$ bulk material and $\text{NFZ}\cdot\text{H}_3\text{PO}_4$ LAG.

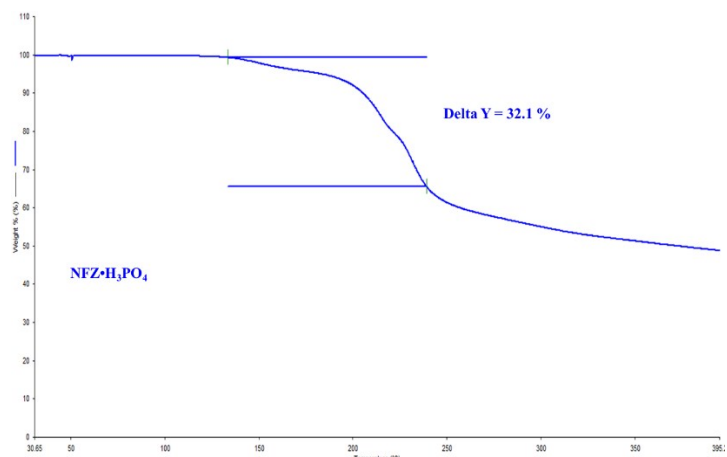


Figure S15. Thermal analysis curve showing weight loss in $\text{NFZ}\cdot\text{H}_3\text{PO}_4$ bulk material.

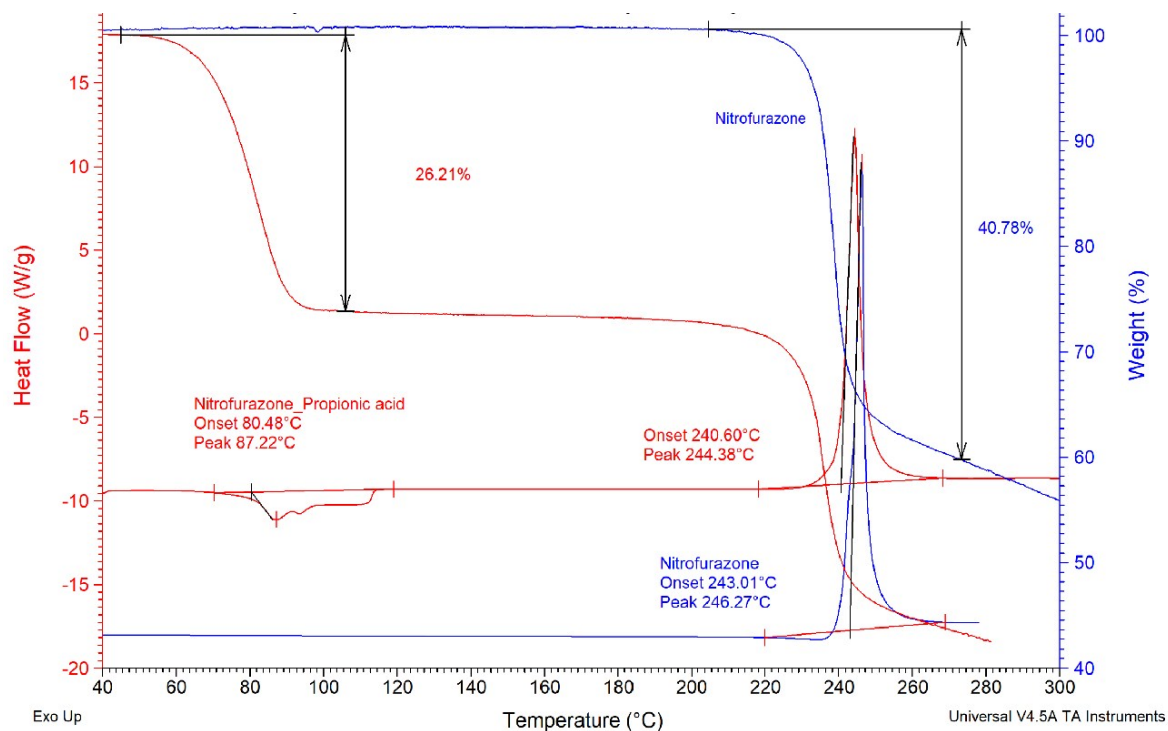


Figure S16. DSC and DTA curves of NFZ•PA.

FTIR analysis of the multicomponent crystals of NFZ

FTIR spectroscopy was used in the comparison of the new crystal structures of NFZ. It is important to note that three species are present in the $4\text{NFZ}\cdot[\text{H}_3\text{O}^+][\text{ClO}_4^-]$ crystal, each possessing unique vibrational modes. Hydrogen bond as well as ionic interactions come into play as they intensify the stiffness of the covalent bonds.¹ Moreover, the ionic species present (i.e. H_3O^+ and ClO_4^-), have a unique symmetry which also influences the overall vibrational frequencies. In this scenario, the tetrahedral (T_d) symmetry of ClO_4^- gives a broad and strong peak at a frequency 1071 cm^{-1} (Figure S17). The trivial lowering is due to $\text{N11-H11}\cdots\text{O20}$ and $\text{C9-H9}\cdots\text{O19}$ intermolecular associations between the anion and the NFZ. Literature also confirms that tetrahedral anions typically have two vibrational modes, that is, symmetric stretching and bending, respectively. Some examples of T_d symmetry anions with their respective stretching and bending vibrational frequencies are as follows: PO_4^{3-} (1017 cm^{-1} , 567 cm^{-1}), CrO_4^{2-} (890 cm^{-1} , 378 cm^{-1}) and MnO_4^- (902 cm^{-1} , 386 cm^{-1}). The 621 cm^{-1} absorption frequency may be attributed to Cl–O asymmetric bending. The C=O frequency has shifted to 1639 cm^{-1} , largely due to the inflexibility of the hydrogen bonded carbonyls.

The other interesting feature of the spectral peaks of $4\text{NFZ}\cdot[\text{H}_3\text{O}^+][\text{ClO}_4^-]$ is the unusually expansive band in the $3600\text{--}3100\text{ cm}^{-1}$ range. This is probably due to the ionized water molecule. The spectral bands of H_2O and H_3O^+ can be difficult to discriminate as their characteristic band range falls in the

same region. Notable differences are seen in the fingerprint region and at peaks 593 and 549 cm^{-1} . The doublet in the starting material's spectrum (blue) seems to have been overshadowed by the broadened absorption band in the crystal spectrum (red). The peak at 3450 cm^{-1} is the N-H stretch of the amine of NFZ and the same group's bending vibrations are shown at 1500 and 1581 cm^{-1} .

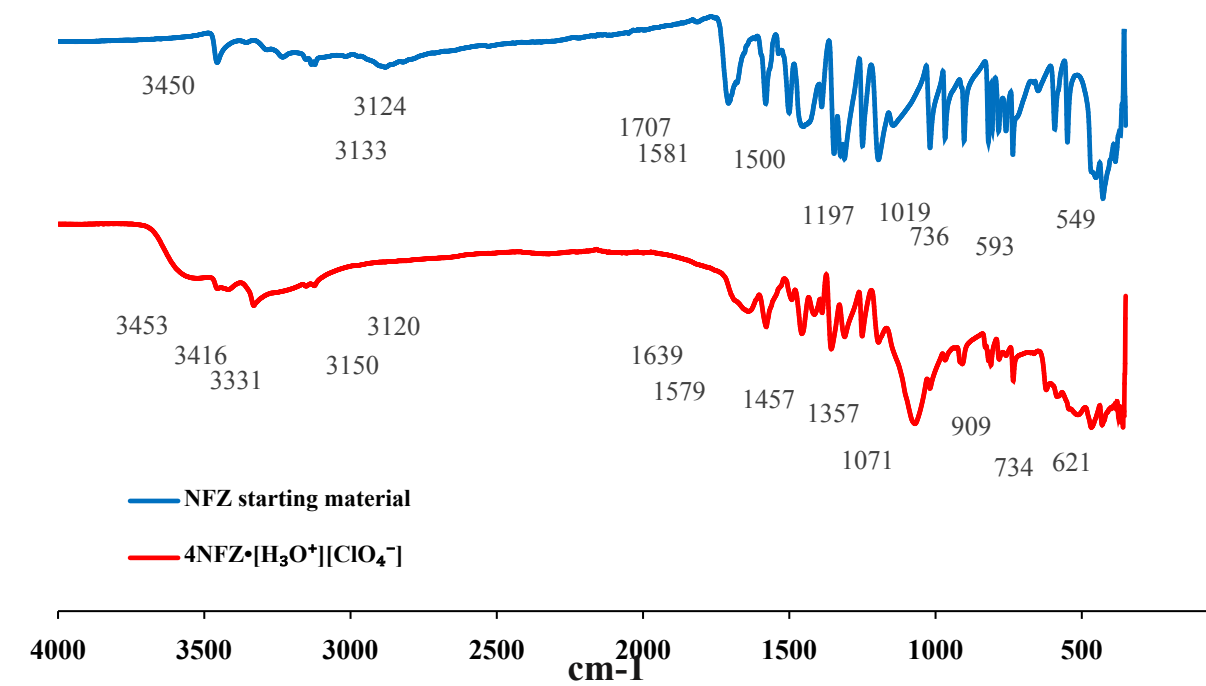


Figure S17. FTIR spectra of NFZ and $4\text{NFZ}\cdot[\text{H}_3\text{O}^+][\text{ClO}_4^-]$.

Vibrational modes of $\text{NFZ}\cdot\text{H}_3\text{PO}_4$ are shown in Figure S18. The broad band in the range of 2700-2550 cm^{-1} is associated with a P(O)OH group of the phosphoric acid.² Literature reports that the broad band in the range of 1100-950 cm^{-1} is associated with aqueous phosphoric acid.³ Since this is in aqueous medium, cannot expect similar absorption band in the case of unprotonated acid in the $\text{NFZ}\cdot\text{H}_3\text{PO}_4$ crystal, but there is room left for anomalous behaviour; the intermolecular interactions may come into play and reduce the vibrational modes by making the P-OH bonds stiffer, thereby affecting the band accordingly. The two peaks at 3470 cm^{-1} and 3367 cm^{-1} are the results of the N-H stretch of the amine of NFZ and the same group's bending vibrations are shown around 1566 cm^{-1}

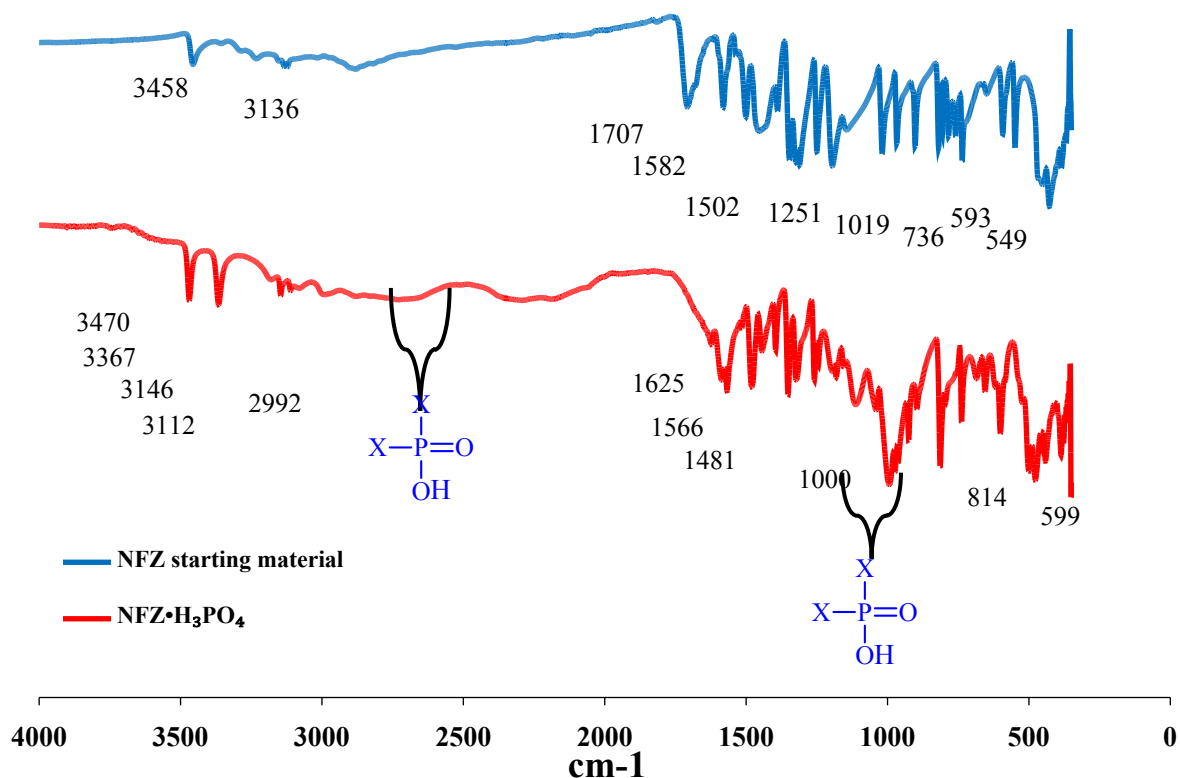


Figure S18. FTIR spectra of NFZ and NFZ•H₃PO₄.

The FTIR spectrum of NFZ•PA is shown on Figure S19. At 3443 cm⁻¹ a small peak represents the N-H and O-H stretches of NFZ and PA, respectively. A neutral carboxyl group with its proton intact shows a sharp C=O stretching band at ca. 1700 cm⁻¹ and a relatively weak sigma bond stretch at approximately 1200 cm⁻¹ if it forms an O-H···N hydrogen bond.⁴ Unlike the example in literature, propionic acid (PA) in the NFZ•PA solvate forms a hydrogen bond with the neutral NFZ tape via O-H···O, and the absorption band is observed at 1689 cm⁻¹. Hydrogen in the latter interaction is more strongly held by the oxygen compared to the less electronegative nitrogen in the former interaction. The O-H covalent bond of the O-H···O becomes stiffer, thus increasing its infrared radiation absorption. This accounts for the lower wavenumber of 1689 cm⁻¹.

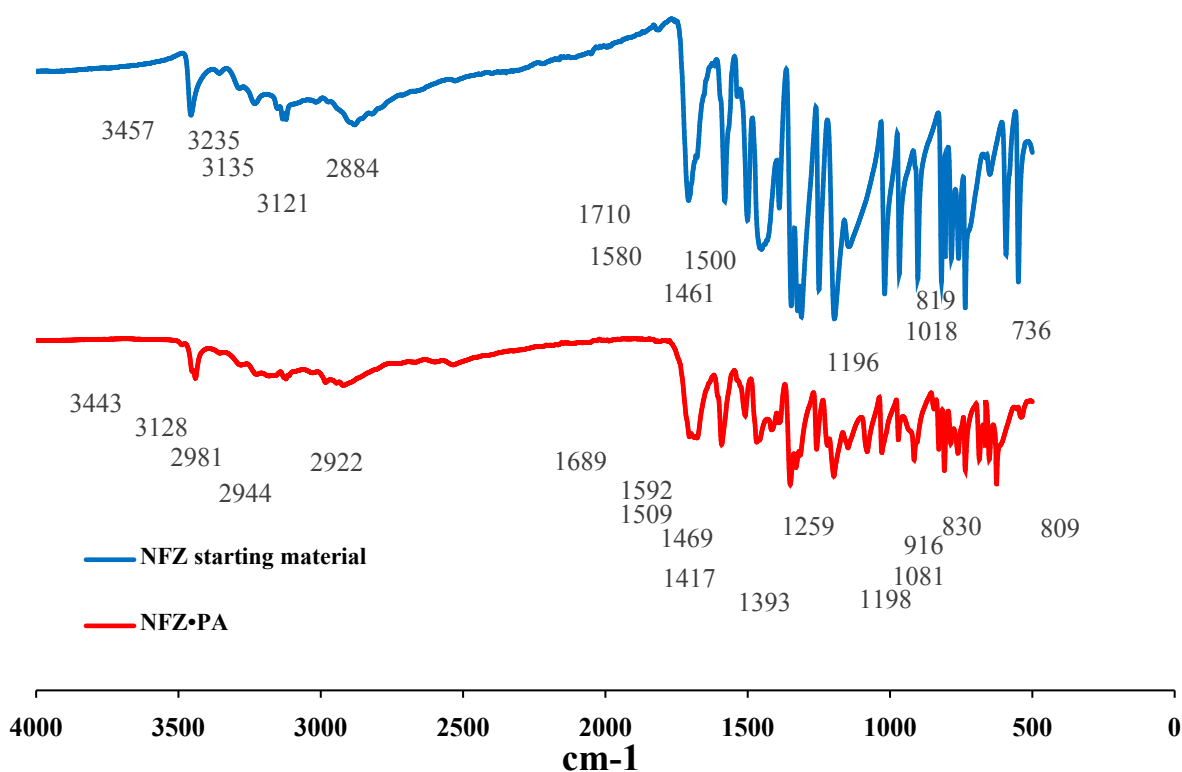


Figure S19. FTIR spectra of NFZ and NFZ•PA.

Materials and methods

All materials were purchased from Sigma-Aldrich and were used without further purifications.

Preparation of Polymorphs of NFZ

Generally, about 2 ml of each solvent was measured using a syringe and added into the vial with NFZ. The solutions were heated at 60°C and stirred for at least 20 minutes to allow the solid to dissolve. Each vial was left to cool to room temperature and the solutions were filtered. The vials were sealed using parafilm and holes were made on the film to allow the slow evaporation of the solvent. All vials were left in a sunlight-free room and kept away from any possible disturbances of crystal growth such as frequent agitations and movements. Some crystals were harvested after a week while others were only collected a month.

Preparation of $4\text{NFZ} \cdot [\text{H}_3\text{O}^+][\text{ClO}_4^-]$ co-crystal salt

Ca. 0.01 g of NFZ was transferred into a vial. 3 ml of 60% HClO_4 (aq) was added into the vial using a glass pipette. The vial was heated and stirred for ca. 60 minutes at 60°C until it completely dissolved.

The yellow solution slowly turned into a deeper colour with time. The vials were left on the bench to cool to room temperature. The vials were filtered after cooling and sealed using parafilm. Holes were made on the film to allow the slow evaporation of the solvent. All vials were left in a sunlight-free room and left unhandled. Reddish brown crystals were harvested after 3 months.

Preparation of NFZ•H₃PO₄ solvate

Ca. 0.01 g of NFZ was transferred into a vial. 3 ml of 3.4% H₃PO₄ (aq) was added into the vial using a syringe. The vial was heated and stirred for ca. 60 minutes at 60°C to allow maximum dissolution. The solution was left on the bench to cool and filtered afterwards. The vials were sealed using parafilm. Holes were made on the film to allow the slow evaporation of the solvent. All vials were left in a sunlight-free room and kept away from any possible disturbances of crystal growth such as frequent agitations and movements. Dark brown crystals were harvested after ca. 4 months.

Preparation of NFZ•PA

Ca. 0.01 g of NFZ was transferred into a vial. About 3 ml of propionic acid was added into the vial using a syringe. The vial was heated and stirred for ca. 60 minutes at 60°C to allow maximum dissolution. The solution was left to cool and filtered afterwards. The vials were sealed using parafilm. Holes were made on the film to allow the slow evaporation of the solvent. All vials were left in a sunlight-free room. Crystals were harvested in about 5 months.

Crystal samples were characterized by various analytical techniques, such as single crystal and powder X-ray diffraction (SCXRD and PXRD), differential scanning calorimetry (DSC), thermo-gravimetric analysis (TGA), hot-stage microscopy (HSM) and Fourier Transform Infra-Red Spectroscopy (FTIR).

Single crystal X-ray diffraction (SCXRD)

A Bruker APEX II DUO X-ray diffractometer using graphite monochromated Mo K α ($\lambda = 0.71073 \text{ \AA}$) radiation was used for data collections. The selected crystal was cooled using an Oxford Cryostream-700 with liquid nitrogen at a flow rate of 20 ml min⁻¹. The X-rays were produced at 50 kV and 30 mA using a Bruker K780 generator. The selected monocrystalline piece was mounted on a cryoloop and covered with Paratone N oil to retain crystallinity. The stream of nitrogen gas was set at 20 ml min⁻¹. Cell refinement and data reduction were carried out using SAINT-Plus.⁵ The X-ray diffraction data were scaled for absorption effects by using SADABS.⁶ The systematic absences found in the X-ray data were studied and used to determine the point group through contrast with known space groups. The value of $|E^2 - 1|$ was also inspected specifically for characteristic centrosymmetric and non-centrosymmetric point groups. The space groups were confirmed using XPREP.⁷

The structure was solved by direct method using the SHELXS program of the SHELXTL package and refined by full-matrix least-squares methods with SHELXL-2014

XPREP was also used to prepare SHELXS data input files which were subsequently used in structure determination using X-Seed.⁸ SHELXS and SHELXL-2014, from the SHELXTL package,⁹ were used to directly solve and refine all structures by using full-matrix least squares against F^2 for unique reflections, where F is the structure factor. Crystal assemblies, information and other figures were generated using Mercury 3.9 software.¹⁰

Powder X-ray diffraction (PXRD)

The Bruker AXS D2 Phaser X-ray Diffractometer was used for analyses. Samples were finely ground and mounted onto a zero-background sample holder. A diffractogram was acquired under ambient conditions at a power setting of 40 kV and 20 mA in reflection mode while the sample oscillated perpendicular to the beam.

Differential Scanning Calorimetry (DSC)

The thermal behaviour of the obtained crystals was recorded with a Perkin Elmer DSC 6000. Crystals taken from the mother liquor were dried with a filter paper and manually crushed. They were placed into a vented aluminium sample pan. The sample sizes were between 2–5 mg and the temperature range typically 25–350°C was at a heating rate of 10–30°C min⁻¹ depending on sample being analysed. The samples were purged with a stream of nitrogen flowing at 20 ml min⁻¹. Calibration was done using Indium as the reference material. A supplementary DTA instrument was used to run one of the crystal samples from an external laboratory. The sample size was between 2-5mg and the temperature range was from 30-300°C.

Thermogravimetric analysis (TGA)

TGA was performed on a Pyris 6 thermogravimetric analyzer. Approximately 3 mg samples were added to an alumina crucible per samples analysed. The samples were heated over a typical temperature range of 30 to 400°C at a heating rate of 10°C min⁻¹. The samples were purged with a stream of flowing nitrogen throughout the experiment at 20 ml min⁻¹. The thermal analysis of NFZ·PA crystals was performed on a TA Q500 instrument from 25 to 400 °C at a heating rate of 10 °C min⁻¹ with a purge gas of dry nitrogen flowing at 60 ml min⁻¹ for comparison of the percentage mass loss with the

expected compound. The crystals were dried on filter paper and placed in an open crucible for thermogravimetric analysis.

Fourier Transform Infra-Red Spectroscopy (FT-IR)

FT-IR spectra were collected from pure samples of the crystals using a Perkin Elmer FT-IR spectrometer UATR TWO equipped with a diamond crystal, operating in the range 350 - 4000 cm^{-1} with a resolution of 4 cm^{-1} and four scans.

Optical microscopy

Optical microscopy analyses were carried out using a Carl Zeiss Discovery V8 Stereo Light Microscope coupled with a digital camera. This enabled the size of the crystals to be determined and recorded.

References

-
- ¹ Du, S.; Wang, Y.; Wu, S.; Yu, B.; Shi, P.; Bian, L.; Zhang, D.; Hou, J.; Wang, J.; Gong, J., Two novel cocrystals of lamotrigine with isomeric bipyridines and in situ monitoring of the cocrystallization. *European Journal of Pharmaceutical Sciences* **2017**.
 - ² Du, S.; Wang, Y.; Wu, S.; Yu, B.; Shi, P.; Bian, L.; Zhang, D.; Hou, J.; Wang, J.; Gong, J., Two novel cocrystals of lamotrigine with isomeric bipyridines and in situ monitoring of the cocrystallization. *European Journal of Pharmaceutical Sciences* **2017**.
 - ³ Kubota, N.; Yokota, M.; Mullin, J. W., The combined influence of supersaturation and impurity concentration on crystal growth. *Journal of Crystal Growth* **2000**, 212, (3), 480-488.
 - ⁴ Shimono, K.; Kadota, K.; Tozuka, Y.; Shimosaka, A.; Shirakawa, Y.; Hidaka, J., Kinetics of co-crystal formation with caffeine and citric acid via liquid-assisted grinding analyzed using the distinct element method. *European Journal of Pharmaceutical Sciences* **2015**, 76, 217-224.
 - ⁵ Bruker, SAINT-Plus (including XPREP), Version 7.12, Bruker AXS Inc, Madison, Wisconsin, USA, 2004.
 - ⁶ Sheldrick, G. M., SADABS. *University of Göttingen, Germany* **1996**.
 - ⁷ Bruker, XPREP, Version 6.14, Bruker AXS Inc, Madison, Wisconsin, USA, 2003.
 - ⁸ Barbour, L. J., X-Seed — A Software Tool for Supramolecular Crystallography. *Journal of Supramolecular Chemistry* **2001**, 1, (4), 189-191.
 - ⁹ Sheldrick, G. M. *SHELXTL* Version 2014/7. <http://shelx.uni-ac.gwdg.de/SHELX/index.php>.
 - ¹⁰ Macrae, C. F.; Edgington, P. R.; McCabe, P.; Pidcock, E.; Shields, G. P.; Taylor, R.; Towler, M.; van de Streek, J., Mercury: visualization and analysis of crystal structures. *Journal of Applied Crystallography* **2006**, 39, (3), 453-457.